THE ASTROPHYSICAL JOURNAL, 340:509–517, 1989 May 1

STELLAR WIND DURING HELIUM NOVA OUTBURST

MARIKO KATO
Department of Astronomy, Keio University
HIDEYUKI SAIO
Department of Astronomy, University of Tokyo
AND
IZUMI HACHISU
Department of Aeronautical Engineering, Kyoto University
Received 1988 July 22; accepted 1988 September 30

ABSTRACT

We have examined the mass ejection process during helium shell flashes on a 1.3 $M_\odot$ white dwarf which accretes pure helium matter. Full cycles of helium shell flashes are followed by two different kinds of approaches: one is a time-dependent hydrostatic calculation, and the other is the construction of the sequence consisting of static models and steady state models with wind mass loss. It is found that a stellar wind occurs if the shell flash is strong enough, i.e., the mass accretion rate is lower than $1.7 \times 10^{-6}\ M_\odot\ \mathrm{yr}^{-1}$.

We have obtained the mass accumulation ratio, i.e., the ratio of the processed matter which remains after a shell flash to the initial envelope mass. This ratio depends strongly on the mass accretion rate $\dot{m}$: it is less than 0.2 for low accretion rates $\dot{m} < 5 \times 10^{-8}\ M_\odot\ \mathrm{yr}^{-1}$, 0.5 for $\dot{m} = 8 \times 10^{-8}\ M_\odot\ \mathrm{yr}^{-1}$, and 0.9 for $\dot{m} = 5 \times 10^{-7}\ M_\odot\ \mathrm{yr}^{-1}$. If the binary size is small enough, further mass loss occurs due to the outer critical Roche lobe overflow. Then the accumulation ratio is fairly reduced. This mass loss seriously affects the existing scenarios on the neutron star formation induced by the accretion.

Subject headings: stars: accretion — stars: binaries — stars: novae — stars: white dwarfs — stars: winds

I. INTRODUCTION

It has been suggested by many authors that neutron stars in some low-mass X-ray binaries and binary radio pulsars are formed through the accretion-induced collapse of white dwarfs (e.g., van den Heuvel 1987; Taam and van den Heuvel 1986 and references therein). Some X-ray binaries (Her X-1, 4U 1626−67, 1E 2259+59, GX 1+4) are believed to have magnetic fields stronger than 10^{11} G to account for their X-ray pulsations. Such strong magnetic fields are also believed to decay to less than 10^{10} G on a time scale of 10^6–10^7 yr. Since the ages of the binary systems Her X-1 and GX 1+4 must be longer than the evolutionary time scale of the low-mass companion, they should be older than 10^9 yr: for Her X-1, the companion is a 2 $M_\odot$ post–main-sequence star, and for GX 1+4, the companion is a low-mass red giant with spectral type M6 IIIe. The other two systems, 4U 1626−67 and 1E 2259+59, are characterized by a 41 minute and a 38 minute orbital period, respectively. They must consist of a neutron star and a low-mass companion (Savonije, de Kool, and van den Heuvel 1986; Taam and van den Heuvel 1986). As for the low-mass binary (radio or X-ray) pulsars, the companion mass is considered to be as small as 1 $M_\odot$ or less. If the iron core collapse occurs in a massive star, the ejected matter exceeds one-half of the total mass of the binary. Then the binary system would be destroyed (Helfand, Ruderman, and Shaham 1983). The ejected mass is expected to be small when the accretion induced collapse of a white dwarf occurs, however. These are the reasons why the neutron stars are considered to form through the accretion-induced collapse of white dwarfs.

Such accretion-induced collapse of a white dwarf is possible under some conditions for a carbon-oxygen (C+O) white dwarf with its initial mass heavier than 1.2 $M_\odot$ and also for an oxygen-neon-magnesium (O+Ne+Mg) white dwarf (see, e.g., reviews by Nomoto 1987*a*, *b* and papers cited therein). In these scenarios there is an important assumption, i.e., the accreting white dwarfs can grow to the Chandrasekhar mass. If the companion star is a low-mass star, the mass transfer is driven by the evolutional envelope expansion, which gives a relatively small mass transfer rate, i.e., $\dot{m} = 10^{-10}$ to $10^{-7}\ M_\odot\ \mathrm{yr}^{-1}$ (e.g., Webbink, Rappaport, and Savonije 1983; Taam 1983). For these mass accretion rates, the hydrogen shell burning on the white dwarf surface is unstable, and, as a result, weak or strong hydrogen shell flashes (nova explosions) occur one after another (Paczyński and Żytokow 1978; Sion, Acierno, and Tomcszyk 1979; Sienkiewicz 1980).

Once a strong nova explosion occurs, a significant part of the envelope mass is ejected from the system (see, e.g., Prialnik 1986). This implies that white dwarfs cannot grow to the Chandrasekhar mass if the mass transfer rate is lower than $\sim 10^{-9}\ M_\odot\ \mathrm{yr}^{-1}$. Kato and Hachisu (1988) demonstrated that wind mass loss occurs for a 1.3 $M_\odot$ white dwarf even in a very weak nova explosion for the mass accretion rate of $\dot{m} \leq 1 \times 10^{-7}\ M_\odot\ \mathrm{yr}^{-1}$. They constructed sequences which consist of steady mass loss and static solutions for one cycle of nova outburst and obtained the mass-loss rate for each stage of the nova cycle. Using the relation between the mass-loss rate and the envelope mass, they further estimated the mass accumulation ratio, i.e., the ratio of the mass which is processed into helium and still remains on the white dwarf to the mass accreted before the ignition.

Kato and Hachisu (1989) have found that such a wind mass loss occurs for relatively massive white dwarfs ($M_{\mathrm{WD}} \gtrsim 0.9\ M_\odot$). They further calculated the mass accumulation ratio for the wide range of the binary parameters taking into account the effect of the outer critical Roche lobe overflow. They concluded that more than 1.1 $M_\odot$ should be transferred from the

companion star in order for a 1.0 $M_\odot$ white dwarf to grow to 1.38 $M_\odot$ even if the mass transfer rate is as high as 1×10^{-7} $M_\odot$ yr^{-1} and the size of the Roche lobe is very large. Therefore, the accretion-induced collapse of white dwarf is unlikely to occur even in a very weak nova.

When the mass accretion rate is higher than $\sim 2 \times 10^{-7}\, M_\odot$ yr^{-1}, the hydrogen shell burning is stable and no nova explosion occurs. The hydrogen-rich matter is steadily processed into helium. The mass accretion rate is limited by some critical value at which the structure of envelope becomes red giant–like (see, e.g., Nomoto 1982). This critical mass accretion rate is $\sim 6 \times 10^{-7}\, M_\odot$ yr^{-1} for relatively heavy (1.2–1.3 $M_\odot$) white dwarfs. Even if hydrogen shell burning is stable, helium shell burning, which ignites after some amount of helium is accreted, is unstable for the helium accretion rate $\dot{m} < 2 \times 10^{-6}\, M_\odot$ yr^{-1} (Kawai, Saio, and Nomoto 1988). Therefore, we must examine the possibility of the wind mass loss during helium shell flashes in order to answer the question whether white dwarfs can grow to the Chandrasekhar mass or not.

Another possibility of accretion-induced collapse is in white dwarf–helium star binary systems (Savonije, de Kool, and van den Heuvel 1986). The formation of such systems is possible in a wide range of the intermediate-mass binary parameters (Tornambé and Matteucci 1986; Iben and Tutukov 1987; Iben *et al.* 1987). In these cases, the direct helium accretion is driven by the gravitational wave radiation, in which the mass accretion rate $\dot{m} \sim 10^{-8}$ to $10^{-7}\, M_\odot$ yr^{-1} is expected. In such accretion rates, helium shell burning is unstable and helium shell flashes occur after a certain amount of helium is accreted on the white dwarf. If the mass loss is negligible during shell flashes, the accretion-induced collapse of white dwarf can be expected. Therefore, it is important to know whether the significant mass loss occurs during helium shell flashes.

Our main purpose in this paper is to determine the mass accumulation ratio when the mass loss occurs during helium shell flashes. To achieve this goal, we first show the existence of wind mass loss solutions for a 1.3 $M_\odot$ white dwarf (§ II) based on Kato's (1983) mass-loss theory. Carefully studying the solutions, we found that the wind mass loss occurs when the photosphere expands to 2.3 $R_\odot$. We cannot, however, conclude from the steady state approach how largely the envelope expands, because we do not know how much nuclear energy is consumed for the envelope matter to climb up against the gravitational potential in the first expansion stage. In order to examine whether the photosphere really expands to 2.3 $R_\odot$ or not, we followed time-dependent evolutions of helium shell flashes using a hydrostatic code (§ III). In this approach we assume that mass loss occurs when the photospheric radius exceeds 1 $R_\odot$. The envelope structures of steady state models are compared with the structures calculated by the time-dependent evolutionary code in § IV. These two structures appear to be in agreement with each other in spite of the two entirely different codes. This implies that our results are fairly reliable. Combining these two calculations, we obtain accurate values of the accumulation ratio, i.e., the ratio of the remaining mass after a shell flash to the initial envelope mass. In § V we summarize this accumulation ratio for various mass accretion rates. Finally, we conclude that our results seriously affect the existing scenarios of accretion-induced collapse of white dwarfs in § VI.

II. OCCURRENCE OF OPTICALLY THICK WIND

We consider a helium shell flash on a helium accreting white dwarf. This is a reduced model of various types of accretion. Direct helium accretion occurs in compact binaries if the companion is a helium star or a helium white dwarf and it fills its inner critical Roche lobe. If the companion is a normal star, the white dwarf accretes hydrogen-rich matter and nuclear burning converts hydrogen into helium on the surface. If the accretion rate is higher than $\sim 2 \times 10^{-7}\, M_\odot$ yr^{-1}, helium steadily piles up on the white dwarf. If the accretion rate is lower than $\sim 1 \times 10^{-7}\, M_\odot$ yr^{-1}, hydrogen shell flashes convert hydrogen into helium intermittently.

Figure 1 shows a schematic diagram of the evolutionary course of a helium nova outburst. The terminology "helium nova" is used to stress the observational aspects of helium shell flashes on a white dwarf surface. This diagram is essentially the same as that of a "hydrogen" nova outburst (Kato and Hachisu 1988). Before the onset of a helium nova, the helium accreting white dwarf stays at point A. When the envelope mass exceeds a critical value, unstable helium burning ignites to trigger a helium shell flash. The star brightens up and goes up in the H-R diagram. The envelope absorbs energy generated by nuclear reactions and expands. Then the star goes redward. If the radius increases enough, mass loss starts at point B due to stellar wind or to the Roche lobe overflow, which depends on the binary parameters as will be explained below. At point C the envelope reaches a thermal equilibrium: the energy generated by nuclear burning balances with the energy loss. After the maximum expansion of the photospheric radius, the star moves blueward while its envelope mass is decreasing. Some envelope mass has been lost from the system when the mass loss stops at point D. After that, the envelope mass gradually decreases due to nuclear

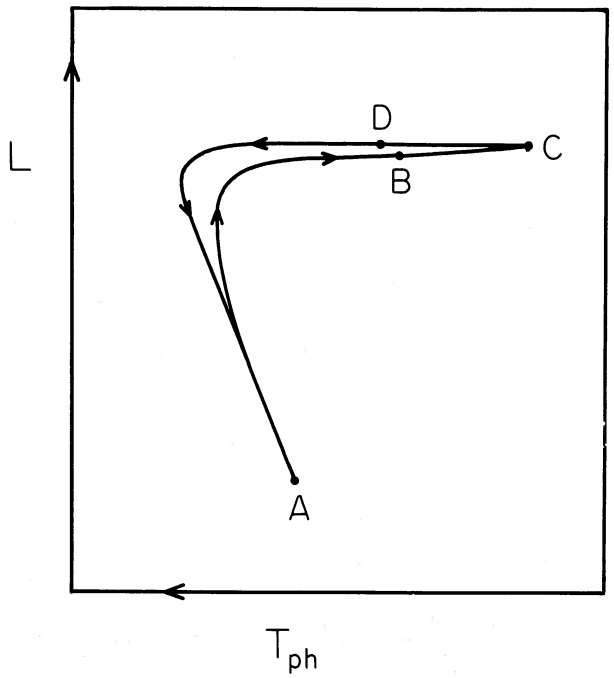

FIG. 1.—A schematic H-R diagram for an evolutionary course of shell flash. An accreting white dwarf stays at point A before the onset of helium shell flash. When the envelope mass reaches a critical value, unstable helium shell burning ignites to trigger a helium nova. Then the star brightens and the envelope absorbs energy generated by nuclear burning and expands greatly. Mass loss starts at point B. After the photospheric radius reaches the maximum value at point C, the envelope reaches a thermal equilibrium. The mass of the helium envelope decreases in time due both to mass loss and to nuclear burning. The mass loss stops at point D.

burning (i.e., the core mass increases) and the star goes blueward. Nuclear burning gradually fades away and the star reaches again point A.

Such an evolutionary path of a helium nova can be followed by a sequence consisting of static models and steady models with mass loss. We use the same assumptions and the same numerical techniques as in Kato and Hachisu (1988), in which a complete cycle of "hydrogen" nova is described for a 1.3 $M_\odot$ white dwarf. The wind is accelerated by continuum radiation, i.e., the so-called optically thick wind. The formulation of the wind and the basic envelope structures are explained in Kato (1983). The envelope is assumed to have a uniform chemical composition of $X = 0$, $Y = 0.97$, and $Z = 0.03$ by mass for hydrogen, helium, and heavy elements, respectively. The radius of the white dwarf core is assumed to be $\log r$ (cm) = 8.513. As for the opacity, we used an analytical formula given by Stellingwerf (1975) for $\log T$ (K) < 6 and by Iben (1975) for $\log T$ (K) > 6. In order to check the error which may come from the opacity formulae, we have calculated additional models using Cox and Tabor's (1976) table for $\log T < 7.5$ and Iben's (1975) formula for $\log T > 7.5$. These two sets of solutions with different opacities give essentially the same results.

Figure 2 depicts evolutionary tracks of one cycle of a helium nova. The evolutionary track in the rising phase (from point A to point C in Fig. 1) depends on the ignition mass: three tracks are plotted for three ignition masses of 6×10^{-5}, 1×10^{-4}, and 1×10^{-3} $M_\odot$, which correspond to the ignition masses at helium accretion rates of $\dot{m} = 1 \times 10^{-6}$, 1.6×10^{-7}, and 4×10^{-8} $M_\odot$ yr^{-1}, respectively (Kato, Saio, and Hachisu 1989). The optically thick wind occurs at the filled circles and terminates at the point with the short vertical bar. Contrary to the initial phase, the evolutionary track in the decay phase (from point C to point A in Fig. 1) is independent of the ignition mass, because the decay phase is assumed to be in the thermal equilibrium.

The envelope mass at point D in Figure 1, where the wind ceases, $\Delta M(D)$, is obtained uniquely as

$$\Delta M(D) = 3.80 \times 10^{-5}\ M_\odot\ . \quad (1)$$

At this phase, the photospheric radius of the envelope is 2.28 $R_\odot$. This envelope mass is important for estimating the amount of mass lost from the system. For instance, if the ignition mass is smaller than this critical value, we roughly expect that no wind would occur.

Models with steady mass loss in the decay phase are plotted by the crosses. The structure of each model with wind mass loss is essentially the same as those of the nova in Kato (1983). The luminosity of the models with mass loss decreases redward in the H-R diagram (Fig. 2) and increases again almost vertically. These properties are also shown in the sequence of a "hydrogen" nova model (see Kato and Hachisu 1989 for the physical explanation).

The mass-loss rate of these wind solutions, $\dot{M}(<0)$, is plotted in Figure 3 against the helium envelope mass ΔM. The mass-loss rate is large when the photospheric temperature is low, and it becomes smaller as the star moves blueward in the H-R diagram.

In our numerical calculations we met difficulties in obtaining models with mass loss in some regions of the H-R diagram where the opacity drastically changes near the surface of the models. In order to check and avoid such difficulties, we used two different ways of obtaining opacities. The circles in Figure 3 denote the solutions in which we use Stellingwerf's analytical opacity, while the triangles correspond to the solutions calculated by using a opacity table in Cox and Tabor (1976). These two sets of opacities give essentially the same results. In the curve of the mass-loss rate, the solid parts correspond to the regions in which no numerical difficulty is encountered. The dashed part corresponds to the region where our numerical method sometimes does not work in the surface region where

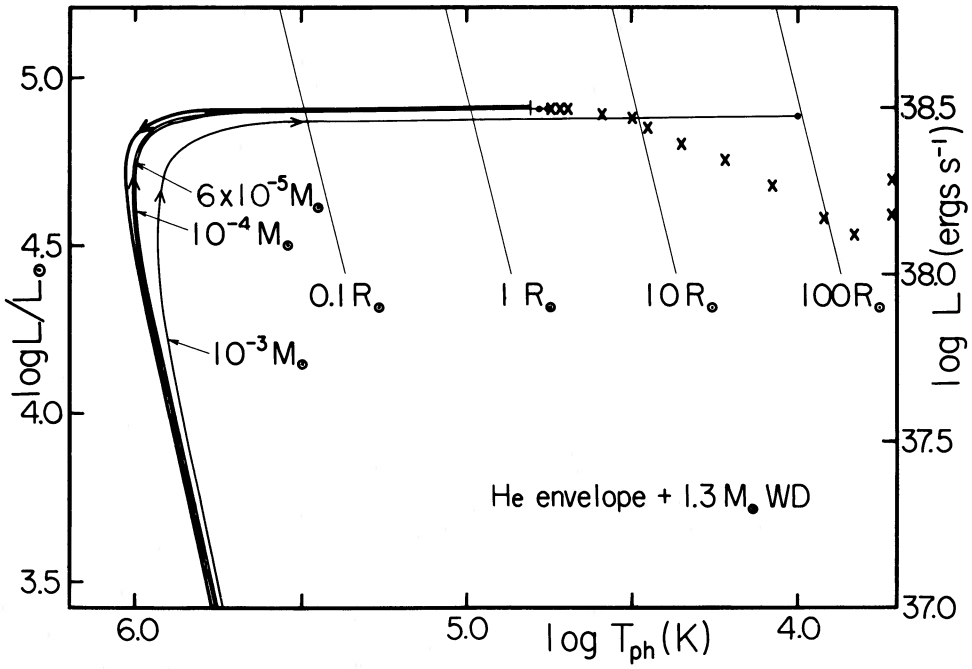

FIG. 2.—One cycle of helium novae based on the static and steady state models. In the rising phase three tracks are shown for three different envelope masses. The wind mass loss occurs at the filled circles. The models with optically thick wind in the decay phase are denoted by the crosses. This wind ceases at the point with short vertical bar. The decay phases of novae are uniquely determined. Thin solid lines denote the constant radius lines.

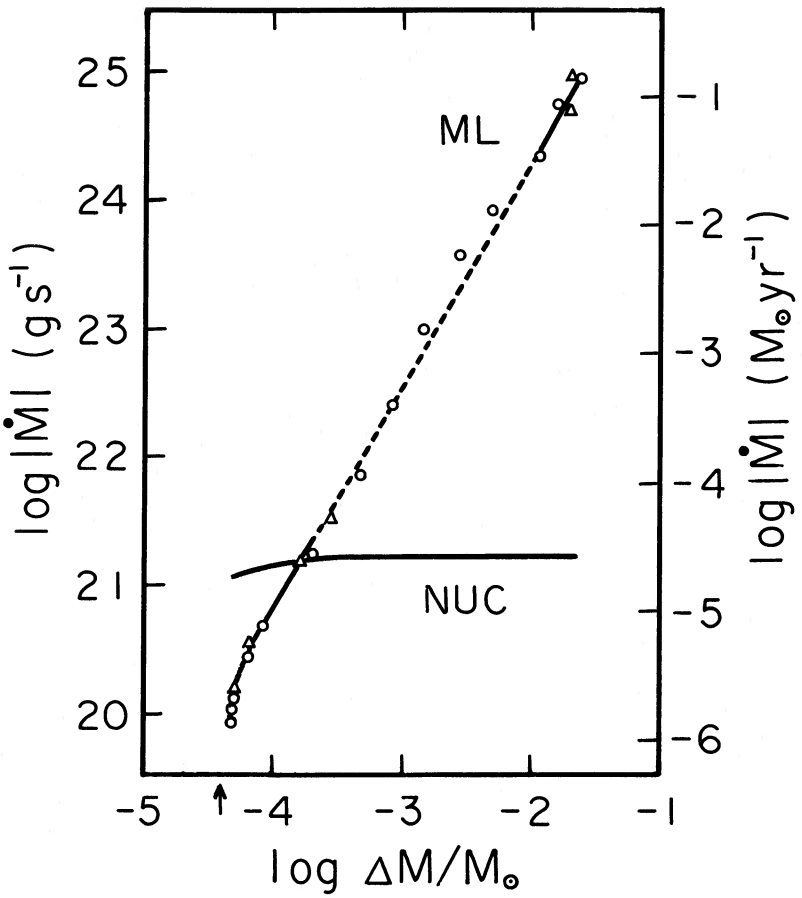

FIG. 3.—The mass-loss rate, $\dot{M}$, of the steady mass-loss solution is plotted against the helium envelope mass ΔM. The mass-loss rates of the wind solutions are denoted by open circles and triangles. Triangles and circles correspond to the solutions with the different formulae of opacity: (*triangles*), Cox and Tabor's (1976) table; (*circles*), Stellingwerf's (1975) formula. The curve marked "NUC" denotes the mass decreasing rate of the envelope by nuclear burning. An arrow indicates the envelope mass at which the wind ceases.

the opacity changes steeply. For these cases, we relaxed the condition of convergence and obtained the closest solution. We hope that these solutions are not far from the real solutions.

The mass-loss rate (in units of $M_\odot$ yr^{-1}) is presented by an empirical formula as follows:

$$\log |\dot{M}| = 1.74 \log (\Delta M/M_\odot) + 2.02 \quad \text{for } \log (\Delta M/M_\odot) \geq -4.1 , \quad (2a)$$

and

$$|\dot{M}| = 0.183(\Delta M/M_\odot - 3.80 \times 10^{-5}) \quad \text{for } -4.42 < \log (\Delta M/M_\odot) < -4.1 . \quad (2b)$$

This formula holds for $-4.42 \leq \log (\Delta M/M_\odot) \leq -1.6$, which corresponds to the range of the mass-loss rate of $-\infty \leq \log |\dot{M}| \leq -0.85$.

III. TIME-DEPENDENT MODELS DURING SHELL FLASHES

As shown in § II, if the radius becomes larger than 2.3 $R_\odot$ during shell flashes, a stellar wind and hence mass loss occur. In other words, the wind mass loss occurs if the helium shell flash is strong enough. It is known that the helium shell flash on an accreting white dwarf is stronger for the lower accretion rate (e.g., Fujimoto and Sugimoto 1982). Although there are some published results of the helium shell flashes (e.g., Taam 1980*a*, *b*; Fujimoto and Sugimoto 1982; Iben 1982), we need the information for the accretion rates different from the previous works, i.e., for accretion rates much higher than theirs. Therefore, we resorted to numerical calculations of the evolutionary models for accreting white dwarfs using the Henyey-type code which was used in Saio and Nomoto (1985).

The outer boundary condition imposed is based on the static envelope in radiative equilibrium (Nomoto and Sugimoto 1974). Since it is very difficult to obtain models by a Henyey-type code when the luminosity is very close to the Eddington luminosity for the electron scattering opacity, we assumed that mass loss starts when the radius exceeds 1 $R_\odot$. The mass-loss rate is arbitrarily set to be $2 \times 10^{-5}\ M_\odot$ yr^{-1}. The results are insensitive to the assumed value of the mass-loss rate as discussed in § VI. Mass loss is replaced with accretion when the radius reduces to 0.02 $R_\odot$. Between 0.03 $R_\odot$ and 0.02 $R_\odot$ the mass-loss rate is gradually reduced. These parameters have been determined by trial and error. If mass loss is replaced by accretion when the radius is much larger than 0.02 $R_\odot$, the luminosity becomes too close to the Eddington luminosity for the outer boundary condition to work properly.

The accretion rates considered are $\dot{m} = 2 \times 10^{-6}$, 1×10^{-6}, 6.6×10^{-7}, 3×10^{-7}, and $1 \times 10^{-7}\ M_\odot$ yr^{-1}, where $6.6 \times 10^{-7}\ M_\odot$ yr^{-1} corresponds to the increasing rate of the helium envelope mass due to the hydrogen shell burning in a

red giant star with a 1.3 $M_\odot$ core (e.g., Nomoto 1982). For the case of $\dot{m} = 2 \times 10^{-6}\ M_\odot\ \mathrm{yr}^{-1}$, the shell flash is too weak for the wind mass loss to occur (the radius is smaller than 1 $R_\odot$), while for the other cases a stellar wind is expected to occur after the peak of the nuclear luminosity. Table 1 summarizes the results of the numerical calculations, which includes the maximum values of the nuclear luminosity, $L_{n,\max}$; the masses of the helium envelope when the mass loss begins, $\Delta M(B)$, and when the mass loss ends, $\Delta M(D)$; the mass accreted in the period from the end of mass loss of the previous shell flash to the beginning of mass loss, $\Delta M_{\rm acc}$; and the lost mass, $\Delta M_{\rm loss}$, where the envelope mass is defined as the mass lying above the mass shell with maximum nuclear energy generation rate.

The initial models adopted are the steady state models, for which the accretion rate is balanced with the nuclear burning rate (Kawai, Saio, and Nomoto 1988). The computations were continued until the shell flashes become approximately limit cycles and the amount of mass loss (if it exists) becomes nearly constant from cycle to cycle. For the case of $\dot{m} = 1 \times 10^{-7}\ M_\odot\ \mathrm{yr}^{-1}$, $\Delta M_{\rm acc}$ and $\Delta M_{\rm loss}$ still tend to increase from cycle to cycle, but the ratios of $\Delta M_{\rm loss}/\Delta M_{\rm acc}$ are nearly constant for the last three flashes. If no mass loss occurs, $\Delta M(B)$ is defined as the helium envelope mass at the phase of the maximum radius.

TABLE 1

PROPERTIES OF TIME-DEPENDENT MODEL

Flash Number	$\log L_{n,\max}$ ($L_\odot$)	$\Delta M(B)$ ($10^{-5}\ M_\odot$)	$\Delta M(D)$ ($10^{-5}\ M_\odot$)	$\Delta M_{\rm acc}$ ($10^{-5}\ M_\odot$)	$\Delta M_{\rm loss}$ ($10^{-5}\ M_\odot$)
$\dot{m} = 2 \times 10^{-6}\ M_\odot\ \mathrm{yr}^{-1}$ (no mass loss)					
1.....	4.41	3.1	...	...	...
2.....	5.48	3.3	...	...	...
3.....	5.08	3.0	...	...	...
4.....	4.82	3.1	...	...	...
5.....	4.64	3.0	...	...	...
$\dot{m} = 1 \times 10^{-6}\ M_\odot\ \mathrm{yr}^{-1}$					
1.....	4.83	2.7	...	...	...
2.....	6.83	5.7	3.1	4.7	0.90
3.....	6.71	6.2	4.0	4.9	1.0
4.....	6.73	6.6	3.3	5.5	1.1
5.....	6.67	6.0	3.1	6.0	1.1
$\dot{m} = 6.6 \times 10^{-7}\ M_\odot\ \mathrm{yr}^{-1}$					
1.....	5.24	2.6	...	...	...
2.....	7.42	7.4	3.0	6.7	2.1
3.....	7.56	9.0	3.3	8.2	2.9
4.....	7.41	8.3	3.6	8.6	3.0
5.....	7.48	8.1	3.6	8.1	3.2
6.....	7.39	8.0	3.5	9.1	3.1
7.....	7.48	8.5	3.4	8.2	3.2
8.....	7.44	8.0	3.5	8.2	3.1
9.....	7.43	7.8	3.1	8.2	3.0
$\dot{m} = 3 \times 10^{-7}\ M_\odot\ \mathrm{yr}^{-1}$					
1.....	6.24	3.5	2.8	0.04	0.01
2.....	8.78	14.4	3.4	14.3	9.4
3.....	8.80	15.4	3.2	16.5	10.1
4.....	8.88	15.6	3.3	16.3	10.4
$\dot{m} = 1 \times 10^{-7}\ M_\odot\ \mathrm{yr}^{-1}$					
1.....	10.28	32.1	...	27.8	28.6
2.....	10.55	40.8	3.6	38.8	34.7
3.....	10.68	43.6	2.9	43.7	38.3
4.....	10.75	46.5	3.2	45.8	40.1
5.....	10.80	47.9	3.0	48.2	42.6

After the mass loss ends and the accretion resumes, the nuclear luminosity L_n, continues to decrease until it attains a minimum value. The minimum value is smaller for the stronger flashes (i.e., the lower accretion rate). When L_n increases to about $10^4\ L_\odot$, a shell convection zone appears above the helium burning shell. The shell convection extends almost throughout the helium envelope when the L_n is nearly maximum. The bottom of the convection zone, where the nuclear energy generation rate is maximum, is located at the bottom of the newly accreted helium envelope. When about one-half of the helium in the envelope is burned, the convective shell disappears. After the disappearance of the convective zone, the radius exceeds 1 $R_\odot$ and mass loss is started. During the mass-loss phase, the envelope mass decreases from $\Delta M(B)$ to $\Delta M(D)$. However, we shall note here that $\Delta M(B) - \Delta M(D) > \Delta M_{\rm loss}$, because during the mass-loss phase the location of the maximum nuclear energy generation rate shifts outward by about $1.8 \times 10^{-5}\ M_\odot$ independent of the mass accretion rate. The helium remaining after the mass loss will be exhausted during the next shell flash without being mixed into the shell convection zone because, as mentioned above, the maximum energy generation occurs at the bottom of the newly accreted helium envelope.

In the case of the highest accretion rate in Table 1 ($\dot{m} = 2 \times 10^{-6}\ M_\odot\ \mathrm{yr}^{-1}$) no mass loss is started, because the photosphere does not reach 1 $R_\odot$ in these weak shell flashes. As mentioned in the previous section, the wind occurs when the envelope expands up to 2.3 $R_\odot$, which is realized if the envelope mass is greater than $3.8 \times 10^{-5}\ M_\odot$. For $\dot{m} = 2 \times 10^{-6}\ M_\odot\ \mathrm{yr}^{-1}$, the envelope mass at the beginning of the shell flash is smaller than this critical value. Therefore no mass loss is expected. In the other cases in Table 1, the envelope mass is larger than the critical value and mass loss occurs. This shows that our two kind of approaches are consistent with each other.

We note that $\Delta M(D)$ shown in Table 1 is smaller than the critical envelope mass for the wind, $3.8 \times 10^{-5}\ M_\odot$, by $(0.5\text{–}0.8) \times 10^{-5}\ M_\odot$, which is caused by the overstripping of the envelope mass because we cannot obtain evolutionary models with nearly Eddington luminosity by our Henyey-type code. So, the actual mass lost by wind is probably smaller than $\Delta M_{\rm loss}$ listed in Table 1 by $(0.5\text{–}0.8) \times 10^{-5}\ M_\odot$.

IV. COMPARISON OF TIME-DEPENDENT AND STEADY STATE MODELS

We have calculated two kinds of models to follow the evolution of helium novae: time-dependent models and sequence of steady state models. Each of our models has merits and drawbacks. The steady state model is excellent in the points that solutions can be obtained even for the luminosity very close to or even exceeding the Eddington luminosity, and that the mass loss rate can be uniquely determined. The drawback to this approach is that we cannot know how much helium has been processed in the rising phase because the ages of the steady state models in the rising phase cannot be obtained. From the steady state models, we can know only that the wind mass loss occurs when the radius expands to some value, but we cannot know exactly whether a real envelope expands to the critical radius.

On the other hand, time-dependent models take into account thermal evolution of the envelope. Therefore, the models tell us whether the envelope can expand to 2.3 $R_\odot$ or not. This approach, however, tends to have a serious difficulty

when the luminosity becomes very close to the Eddington luminosity. Combining these complementary approaches, we get a lot of information about helium nova explosion.

First, we compare the tracks in the H-R diagram. Figure 4 shows a complete cycle of evolutionary models for $\dot{m} = 6.6 \times 10^{-7}\ M_\odot\ \mathrm{yr}^{-1}$ and $3 \times 10^{-7}\ M_\odot\ \mathrm{yr}^{-1}$. The luminosity in the expanding phase is lower than that in the shrinking phase for a given effective temperature. This difference in luminosity is larger for the lower accretion rate (the stronger flashes). The plateau luminosity for the shrinking phase does not depend on the accretion rate. These properties and the absolute values of luminosity for a given effective temperature agree well with those of the sequence consisting of steady state solutions in § II.

The entropy distributions, as an example of the local physical quantities of the solutions, are shown as functions of the distance from the center in Figure 5 for some selected models. The solid and the broken lines correspond to the steady state and the evolutionary models, respectively. Short bars indicate the loci of the photospheres. These figures show that the envelope structures of the two different models are more or less in agreement with each other. Therefore, we can conclude that our two approaches give essentially the same results.

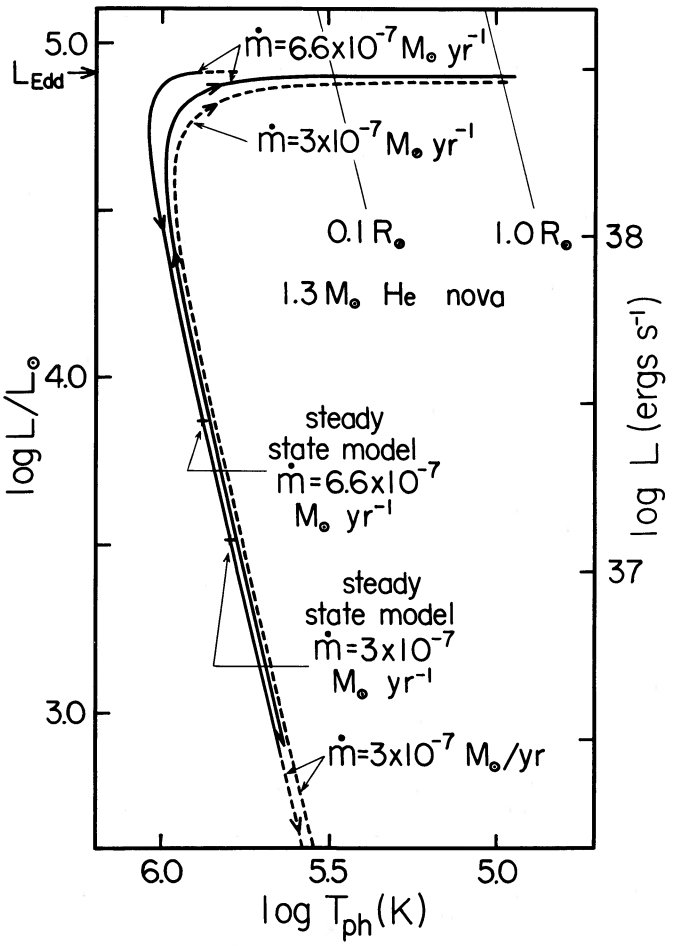

FIG. 4.—The H-R diagram of evolutionary models. Two different cycles are plotted for two different mass transfer rates, $\dot{m} = 3 \times 10^{-7}$ (*dashed curve*) and $\dot{m} = 6.6 \times 10^{-7}\ M_\odot\ \mathrm{yr}^{-1}$ (*solid curve*). The Eddington luminosity corresponding to the 1.3 $M_\odot$ white dwarf for the electron scattering opacity is denoted by an arrow.

V. MASS ACCUMULATION RATIO

During a helium nova, a significant part of the initial envelope mass may be blown off. In this section we will estimate how much mass is lost from the system, or in other words, how much mass accumulates on the white dwarf. We estimate the accumulation ratio based on the wind solutions. Next, we compare it with the direct results from the evolutional models.

a) Mass Accumulation Ratio of Wind Solutions

In this subsection, we consider the mass loss only by the wind. This corresponds to a binary having a very large separation. In the sequences consisting of mass loss and static models, we have assumed that the envelope mass decreases due both to the optically thick wind and to nuclear burning. After the wind ceases (after point D in Fig. 1), the envelope mass decreases due only to nuclear burning. We define the accumulation ratio, η, which is the ratio of the mass is converted into the core material, ΔM_{nuc}, to the initial envelope mass ΔM_i, i.e.,

$$\eta = \Delta M_{\mathrm{nuc}}/\Delta M_i\ . \tag{3}$$

A helium shell flash occurs when the envelope mass reaches ΔM_i. In the rising phase, nuclear burning converts helium into carbon-oxygen mixture, but it is mixed throughout the envelope by convection. Therefore, we assume that the processed matter does not accumulate on the white dwarf at least in this rising phase. We further assume that the envelope quickly reaches a thermal equilibrium (point C in Fig. 1). In other words, we assume that the envelope mass is still ΔM_i when it reaches point C. Then the mass-loss rate is calculated from Figure 3. The decreasing rate of the envelope mass due to nuclear burning is obtained from

$$\dot{M}_{\mathrm{nuc}} = L_n/\epsilon Y\ , \tag{4}$$

where L_n is the nuclear luminosity and $\epsilon = 6 \times 10^{17}$ ergs g^{-1} is the nuclear energy generation per unit mass by helium burning. We assume $Y = 0.5$ in equation (4) because it is known from the time-dependent models that a significant amount of helium has been processed in the initial convective phase. The envelope mass decreasing rate by nuclear burning is also plotted in Figure 3 (the solid line marked "NUC"). The amount of mass processed in the wind phase, $\Delta M_{\mathrm{nuc,\,CD}}$, is obtained as

$$\Delta M_{\mathrm{nuc,\,CD}} = \int_{\Delta M(D)}^{\Delta M_i} \dot{M}_{\mathrm{nuc}}/(|\dot{M}| + \dot{M}_{\mathrm{nuc}})d(\Delta M)\ . \tag{5}$$

After the wind ceases, the envelope mass decreases due only to nuclear burning. According to the time-dependent calculations (§ III), we may assume that all of the mass $\Delta M(D)$ accumulates on the white dwarf, i.e.,

$$\Delta M_{\mathrm{nuc}} = \Delta M_{\mathrm{nuc,\,CD}} + \Delta M(D)\ . \tag{6}$$

We use the ignition mass calculated by Kato, Saio, and Hachisu (1988) as the initial envelope mass, ΔM_i, in equation (3). Substituting equation (6) into equation (3), we obtain the accumulation ratio when the size of the Roche lobe is very large. Figure 6 depicts the mass accumulation ratio, η, against the mass transfer rate $\dot{m}$: the solid curve marked "∞". The accumulation ratio is large for high accretion rates because the ignition mass is small for high accretion rates.

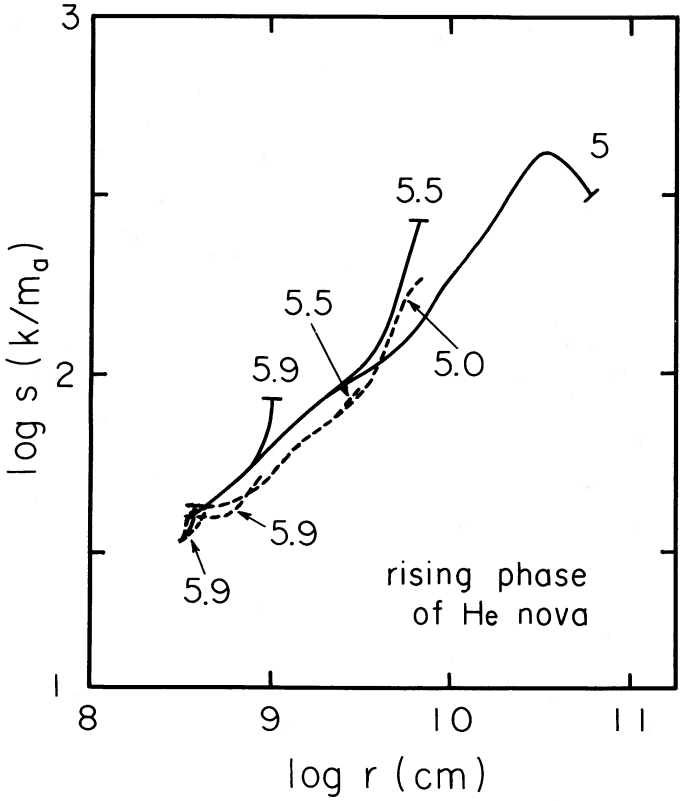

FIG. 5a

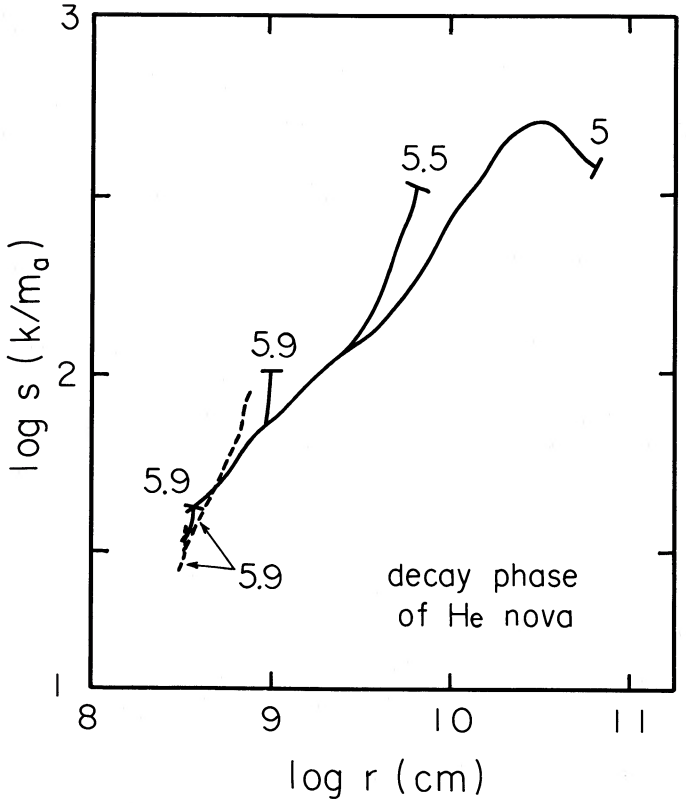

FIG. 5b

FIG. 5.—The entropy distributions vs. the radial coordinate. The solid and the dashed curves denote the structures of the steady state and the evolutionary models, respectively. Logarithmic surface temperatures are attached to each curve. (*a*) The rising phase of helium nova; (*b*) the decay phase.

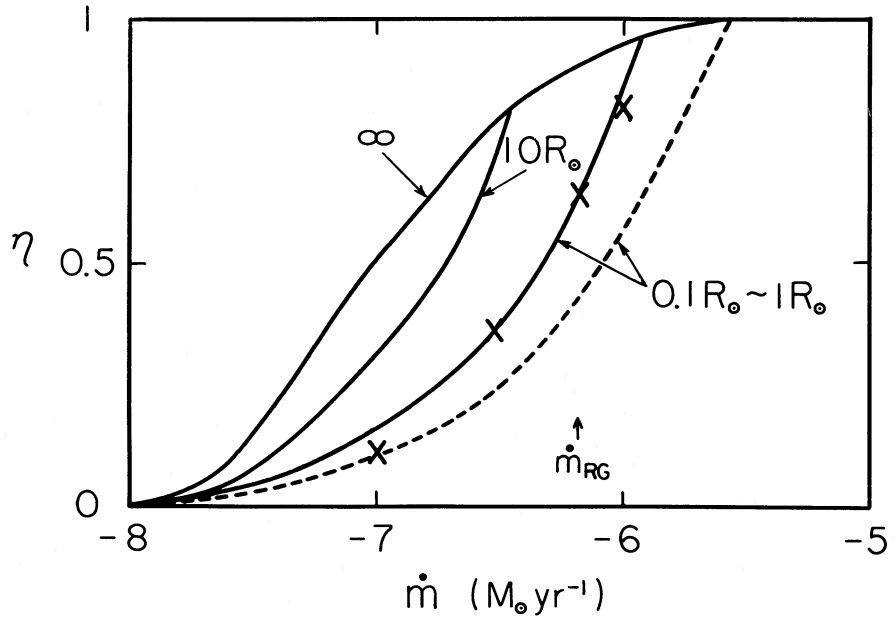

FIG. 6.—The accumulation ratio, i.e., the ratio of the processed matter accumulated on the white dwarf to the mass transferred from the companion star before the ignition, is plotted against the helium accretion rate, $\dot{m}$. The crosses denote the mass accumulation ratio obtained directly from the evolutionary models. The ratio obtained by the steady state calculations are denoted by the solid curves. The dashed curve denotes the ratio without including the effect of the shift of the nuclear burning shell during the outer critical Roche lobe overflow phase. The size of the outer critical Roche lobe is attached to each curve.

b) Outer Critical Roche Lobe Overflow

If the size of the outer critical Roche lobe is small enough, the Roche lobe overflow comes into effect. When the envelope expands greatly, matter outside the outer critical Roche lobe is accelerated by gravitational torque and will finally be lost from the system (e.g., Sawada, Hachisu, and Matsuda 1984). This mass loss by the outer critical Roche lobe overflow is faster than the wind if the separation is relatively small; then we may assume that the matter outside the outer critical Roche lobe is quickly removed from the system.

The mass accumulation ratio of this case is estimated as follows: When we assume that the rate of mass loss by the outer critical Roche lobe overflow is much faster than $\dot{M}_{\rm nuc}$, if the size of the Roche lobe is larger than 2.3 $R_\odot$, the mass loss by the stellar wind ensues even after the Roche lobe overflow has stopped. Then, we must change the beginning point of the integration of the envelope mass, $\Delta M_{\rm nuc,\,CD}$, in equation (5). Instead of ΔM_i, we take the envelope mass just when the photospheric radius of the envelope equals to the outer critical Roche lobe. If the size of the Roche lobe is smaller than 2.3 $R_\odot$, no wind occurs after the outer critical Roche lobe overflow stops. Then, we drop the first term in the right-hand side of equation (6). The second term is replaced by the envelope mass of the static solution which just fills up the outer critical Roche lobe. The accumulation ratio obtained in this way is plotted in Figure 6 (*dashed lines*) against the mass transfer rate, $\dot{m}$, for three different sizes of the outer critical Roche lobe, i.e., 0.1 $R_\odot$, 1 $R_\odot$, and 10 $R_\odot$. The mass accumulation ratios for 0.1 and 1 $R_\odot$ are almost the same because the envelope mass is insensitive to the radius on the plateau part in the H-R diagram as long as the static solutions are concerned.

c) Comparison with the Results of the Time-dependent Models

In the time-dependent models, we have assumed that the mass loss begins when the envelope radius exceed about 1 $R_\odot$ because of the numerical difficulty. This can be regarded that the size of the outer critical Roche lobe is 1 $R_\odot$. The accumulation ratio is calculated directly by $\eta = 1 - \Delta M_{\rm loss}/\Delta M_{\rm acc}$ for this case. These values are also plotted in Figure 6 by crosses. These results corresponds to the overflow from the outer critical Roche lobe with a size of 0.1–1.0 $R_\odot$. For the mass accumulation ratios shown by the dashed line in Figure 6 for 0.1 $R_\odot$ and 1.0 $R_\odot$, the decrease in the envelope mass due to helium burning is not included because the Roche lobe overflow is assumed to be very fast. On the other hand, in the time-dependent models the location of the maximum energy generation moves outward by $\sim 1.8 \times 10^{-5}\ M_\odot$ (i.e., envelope mass decreased by this amount other than mass loss) during the mass-loss phase (§ III). If this effect is applied to the dashed line for 0.1–1.0 $R_\odot$ in Figure 6, the accumulation ratio shifts to the solid line, which agrees very well with the results of the time-dependent models (*crosses*). The little difference is explained by the fact that we have overestimated $\Delta M_{\rm loss}$ in the evolutional model by (0.5–0.8) $\times 10^{-5}\ M_\odot$ as explained in § III.

VI. DISCUSSION AND CONCLUDING REMARKS

In the time-dependent calculations, we have assumed that the mass loss occurs when the radius exceeds 1 $R_\odot$ and we have chosen an arbitrary value for the mass-loss rate. In order to check the sensitivity of the results to the mass-loss rate arbitrarily chosen by us, we have recomputed the last one or two flash cycles by changing the mass-loss rate for the case of $\dot{m} = 6.6 \times 10^{-7}\ M_\odot\ {\rm yr}^{-1}$. No appreciable changes in $\Delta M_{\rm loss}$ were observed for the maximum mass-loss rates ranging from 2×10^{-5} to $1 \times 10^{-4}\ M_\odot\ {\rm yr}^{-1}$. If the mass loss is started when the photospheric radius, $R_{\rm ph}$, reaches 0.03 $R_\odot$ and it is stopped when $R_{\rm ph} = 0.02\ R_\odot$, which is likely to occur for double white dwarf systems, we obtained $\Delta M_{\rm loss} = 3.1 \times 10^{-5}\ M_\odot$. If the mass loss continues until the radius reduces to 0.01 $R_\odot$, we obtain $\Delta M_{\rm loss} = 3.6 \times 10^{-5}\ M_\odot$. Thus, the amount of the lost mass during the helium shell flashes is insensitive to the artificial treatment of the mass loss. This is due partially to the fact that the envelope mass of the equilibrium models is insensitive to the radius of the envelope (i.e., the radius is very sensitive to the envelope mass) once the envelope expands to the plateau branch in the H-R diagram.

We examined the mass ejection process during helium shell flashes. Our results demand some modifications in the argument of the accretion-induced collapse of white dwarfs. For example, Savonije, de Kool, and van den Heuvel (1986) studied the evolution of a binary consisting of a heavy white dwarf and a low-mass helium star to account for the evolution of the compact neutron star–helium white dwarf binary 1E 2259+586. Assuming conservative mass transfer, they concluded that the heavy white dwarf becomes a neutron star through the accretion-induced collapse of white dwarf. However, our results indicates that their assumption of no systemic mass loss is not justified. Since the mass transfer is driven by the gravitational wave radiation in these white dwarf–helium star systems, its mass transfer rate is relatively small, i.e., $\dot{m} \sim 10^{-8}$ to $10^{-7}\ M_\odot\ {\rm yr}^{-1}$. The size of the outer critical Roche lobe is as small as 1 $R_\odot$ or less and then at least 90% of the accreted helium envelope mass is blown off the system due both to wind mass loss and to the outer critical Roche lobe overflow. Thus, the possibility of the accretion-induced collapse of heavy white dwarfs must be studied carefully.

We would like to thank K. Nomoto for discussions. One of us (I. H.) thanks Joel E. Tohline for the hospitality at LSU. This research has been supported in part by the Japanese Ministry of Education, Science, and Culture through research grant 63740135, by the Space Data Analysis Center, Institute of Space and Astronautical Sciences, and by the United States National Science Foundation grant AST-8701503. The numerical calculations were carried out on Hitachi M-680H at the Computer Center of the University of Tokyo, on Fujitsu M780/VP200 at the Data Analysis Center of the Institute of Space and Astronautical Science, and on VAX8600 at JILA.

REFERENCES

Cox, A. N., and Tabor, J. E. 1976, *Ap. J. Suppl.*, **31**, 271.
Fujimoto, M. Y., and Sugimoto, D. 1982, *Ap. J.*, **257**, 291.
Helfand, D. J., Ruderman, M. A., and Shaham, J. 1983, *Nature*, **304**, 423.
Iben, I., Jr. 1975, *Ap. J.*, **196**, 547.
———. 1982, *Ap. J.*, **259**, 244.
Iben, I. Jr., Nomoto, K., Tornambé, A., and Tutukov, A. V. 1987, *Ap. J.*, **317**, 717.
Iben, I. Jr., and Tutukov, A. V. 1987, *Ap. J.*, **313**, 727.
Kato, M. 1983, *Pub. Astr. Soc. Japan*, **35**, 507.
Kato, M., and Hachisu, I. 1988, *Ap. J.*, **329**, 808.
———. 1989, *Ap. J.*, submitted.
Kato, M., Saio, H., and Hachisu, I. 1989, in preparation.
Kawai, Y., Saio, H., and Nomoto, K. 1988, *Ap. J.*, **328**, 207.
Nomoto, K. 1982, *Ap. J.*, **253**, 798.
———. 1987*a*, in *IAU Symposium 125, The Origin and Evolution of Neutron Stars*, ed. D. J. Helfand and J.-H. Huang (Dordrecht: Reidel), p. 282.
———. 1987*b*, in *13th Texas Symposium on Relativistic Astrophysics*, ed. M. P. Ulmer (Singapore: World Scientific), p. 519.

Nomoto, K., and Sugimoto, D. 1974, *Pub. Astr. Soc. Japan*, **26**, 129.
Paczyński, B., and Żytokow, A. N. 1978, *Ap. J.*, **222**, 604.
Prialnik, D. 1986, *Ap. J.*, **310**, 222.
Saio, H., and Nomoto, K. 1985, *Astr. Ap.*, **150**, L21.
Savonije, G. J., de Kool, M., and van den Heuvel, E. P. J. 1986, *Astr. Ap.*, **155**, 51.
Sawada, K., Hachisu, I., and Matsuda, T. 1984, *M.N.R.A.S.*, **206**, 673.
Sienkiewics, R. 1980, *Astr. Ap.*, **95**, 295.
Sion, E. M., Acierno, M. J., and Tomcszyk, S. 1979, *Ap. J.*, **230**, 832.
Stellingwerf, R. F. 1975, *Ap. J.*, **195**, 441; erratum 1975, *Ap. J.*, **199**, 705.
Taam, R. E. 1980*a*, *Ap. J.*, **237**, 142.
———. 1980*b*, *Ap. J.*, **242**, 749.
———. 1983, *Ap. J.*, **270**, 694.
Taam, R. E., and van den Heuvel, E. P. J. 1986, *Ap. J.*, **305**, 235.
Tornambé, A., and Matteucci, F. 1986, *M.N.R.A.S.*, **223**, 69.
van den Heuvel, E. J. P. 1987, in *IAU Symposium 125, The Origin and Evolution of Neutron Stars*, ed. D. J. Helfand and J.-H. Huang (Dordrecht: Reidel), p. 393.
Webbink, R. F., Rappaport, S., and Savonije, G. J. 1983, *Ap. J.*, **270**, 678.

IZUMI HACHISU: Department of Aeronautical Engineering, Kyoto University, Kyoto 606, Japan

MARIKO KATO: Department of Astronomy, Keio University, Kouhoku-ku, Yokohama 223, Japan

HIDEYUKI SAIO: Department of Astronomy, Faculty of Science, University of Tokyo, Bunkyo-ku, Tokyo 113, Japan